Hydrothermal liquefaction of Elaeis guineensis trunks

Lessons learned from a case study in Guatemala

Cutz, Luis; Maldonado de León, H.A.; Zambrano, Gamaliel; Al-Naji, Majd; de Jong, Wiebren

DOI
10.1016/j.indcrop.2023.117552

Publication date
2023

Document Version
Final published version

Published in
Industrial Crops and Products

Industrial Crops & Products 206 (2023) 117552

Contents lists available at ScienceDirect

Industrial Crops & Products

journal homepage: www.elsevier.com/locate/indcrop

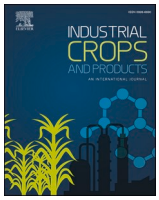

Hydrothermal liquefaction of Elaeis guineensis trunks: Lessons learned from a case study in Guatemala

Luis Cutz [a,*,1], Héctor Maldonado [a,b,1], Gamaliel Zambrano [c], Majd Al-Naji [d], Wiebren de Jong [a]

[a] Process and Energy Department, Delft University of Technology, Leeghwaterstraat 39, 2628 CB Delft, the Netherlands
[b] Biotechnology Department, Delft University of Technology, Van der Maasweg 9, 2629 HZ Delft, the Netherlands
[c] Centro de Procesos Industriales e Ing. Química, Universidad del Valle de Guatemala, Guatemala
[d] BasCat - UniCat BASF JointLab, Technische Universität Berlin, Hardenbergstraße 36, Sekr. EW K-01, Berlin 10623, Germany

ARTICLE INFO

Keywords:
Hydrothermal liquefaction
Bio-oil
Biomass
Oil palm residues

ABSTRACT

The oil palm industry has been under public scrutiny during the last decades due to environmental and social issues related to its practices. Oil palm (*Elaeis guineensis Jacq.*) trunks (OPTs) are of special interest as they are left idle in the field after the replanting process which is performed every 25 years. This common practice results in harvesting challenges, phytosanitary risks, and a loss of bioenergy potential. Due to their high moisture content and fibrous nature, OPTs present a problem for traditional conversion processes that require a dry and homogeneous material. This study evaluates the feasibility of converting OPTs into a bio-crude oil and biochar to increase the sustainability of the oil palm sector. To date, research efforts have primarily focused on hydrothermal liquefaction (HTL) of OPT without catalysts, resulting in a limited understanding of the potential of OPTs. Thus, the main novelty of this work is the evaluation of the effects of catalyst dosage (0–5 wt%) on the bio-oil yield, reaction temperature (260–300°C), and residence time (15–60 min) using a half-fraction experimental design methodology. For this, OPTs extracted from two plantations in Guatemala were used. The maximum bio-oil yield (26.77 ± 3.60 wt%) was found at 260°C for 15 min and 5 wt% catalyst with a high heating value (HHV) of 19.29 ± 1.33 MJ kg^{-1}. Nonetheless, the bio-oils produced without a catalyst at 300°C and 15 min have higher HHV (27.63 ± 1.35 MJ kg^{-1}) and are similar to Diesel fuel based on their H/C and O/C ratio. These results indicate that there is a potential trade-off between the bio-crude oil mass yield and HHV when using the catalyst.

1. Introduction

Currently, mankind faces global challenges at an unprecedented extent due to anthropogenic climate change such as land degradation, biodiversity loss, and excessive use of fossil fuels. This has motivated all sectors to set measures to adapt to a changing climate and work on innovations that can facilitate the transition to a fossil-free economy. When it comes to large and far-reaching transportation, biofuels are suggested as a way to cut emissions, but their sustainability has been questioned when they are made from first-generation feedstocks.

First-generation biofuel feedstocks including vegetable oil crops have raised concerns due to their rapid expansion on agricultural land and environmental impact (Oettli et al., 2018). Among the major vegetable oils are crude palm oil (*Elaeis guineensis Jacq.*) and palm kernel oil, accounting together for around 40% of the global demand for food, animal feed, and biodiesel (Oettli et al., 2018; Meijaard et al., 2020). This is because oil palm has one of the highest oil yields compared with other oil crops and is often economically viable on land unsuitable for most other crops (Meijaard et al., 2020). Unfortunately, there is a long documented history of environmental, political, and social problems associated with the palm oil sector worldwide (Hervas, 2021; Teng et al., 2020; Murphy et al., 2021). With the intention to improve current practices, the Roundtable on Sustainable Palm Oil (RSPO) aims to promote the cultivation of palm oil in a responsible manner that safeguards the environment, local communities, workers, and biodiversity. In this regard, the latest studies indicate that the expansion of palm oil to irrigated tropical grassy and dry forest biomes could be in compliance with the zero-deforestation commitments (ZDCs) made by many companies (Fleiss et al., 2023). Thus, given the expected growth of the palm oil sector, it is crucial to investigate if there are innovative approaches to boost its circularity and lessen its environmental impact.

* Corresponding author.
E-mail address: Luis.Cutz@tudelft.nl (L. Cutz).
[1] These authors have equally contributed to this work.

https://doi.org/10.1016/j.indcrop.2023.117552
Received 21 June 2023; Received in revised form 10 September 2023; Accepted 21 September 2023
Available online 11 October 2023

Nomenclature

Abbreviations

Abbreviation	Definition.
AQ	Aqueous phase.
at.	atomic.
BC	Biochar.
BOPT	Bio-oil fraction from oil palm trunks.
cat	Catalyst or catalytic.
daf	Dry ash free basis.
d.b.	Dry basis.
DCM	Dichloromethane.
DOE	Design of experiments.
GREPALMA	Guild of Palm Growers of Guatemala (in Spanish).
HTL	Hydrothermal liquefaction.
HHV	Higher heating value.
OPT	Oil palm trunk(s).
SER	Standard error of regression.
UVG	University of the Valley of Guatemala.
w.b.	Wet basis.

Symbols

Symbol	Definition Unit.
T	Temperature ˚C.
t	Reaction time min.
V	Volume m^3.
w	Weight g.
X	Coefficient -
Y	Mass yield wt%.

Subscripts

0	Reference or intercept.
aq	Aqueous phase.
G	Gas.

This question is addressed in the context of Guatemalan palm oil plantations. According to the Guild of Palm Growers of Guatemala (GREPALMA), Guatemalan palm oil plantations have a number density of 143 palms per hectare occupying about 1500 km^2 - about 4% of the arable land (Castellanos et al., 2017). Furthermore, plantations must be renovated around every 25 years. In Guatemala, the oldest plantations can be traced back to the ’90 s in the southern region. The renovation of palm oil plantations in Guatemala is done using a method called “underplanting". This method consists of injecting herbicide into the old palm (about 13 m high) so the palm drops its fronds and the trunk remains. Then, a new palm is planted next to the trunk of the previous one (United Nations Environment Programme, 2012). This strategy has proved to be detrimental to the growth rate of new palms and creates a breeding ground for pests (United Nations Environment Programme, 2012; Ooi, 2004). According to data reported in 2017 for Guatemala (Castellanos et al., 2017), at the peak of renovation of a particular plantation, an estimate of 772 ktons per annum (ktpa) of biomass from these trunks would be left on the fields. These residues have the potential to be converted into biofuels (Muda et al., 2019) and thus contributing to improving the sustainability of the sector. In Guatemala, the most serious concerns about the palm oil sector are evictions carried out through violence, mistreatment of employees, disruption to the traditional peasant food system and it does not create enough jobs or generate adequate local prosperity (Hervas, 2021; Teng et al., 2020; Mingorría et al., 2014). Due to the crop’s importance to Guatemala’s economy and the lack of better alternatives to replace oil palm products, the palm oil sector and its stakeholders must work harder to improve current procedures and help the country achieve a more sustainable future. At the moment, the only biofuel produced at a large scale in Guatemala is bioethanol, yet no domestic market appears to be in the near future (Cutz et al., 2020).

Biofuels can be produced by various routes such as chemical, thermochemical, and biochemical conversion (Williams et al., 2020). Within the thermochemical processes, HTL has proved to be useful for converting highly heterogeneous and high moisture-content materials into biofuels. For example, forest residues, agricultural residues, food waste, and even waste plastic (Durak, 2023; Gollakota et al., 2018; Helmer Pedersen and Conti, 2017. This process consists of treating the material in an aqueous environment at a relatively mild temperature (150–400˚C) and pressure (5–25 MPa) (Zhang, 2010. When dealing with organic feedstocks, HTL converts biomass into four fractions: bio-oil, biochar, aqueous phase, and gaseous phase.

Research on the valorization of OPTs via HTL is scarce (Muda et al., 2019) and to the best of the author’s knowledge non-existent when using catalysts. Muda et al., evaluated the effect of temperature, residence time, and different sections of the trunks on the HTL process. From their results, the optimum reaction time and temperature that maximize the bio-oil yield were identified. However, it must be noted that the study was conducted using a one-factor-at-a-time (OFAT) methodology. The OFAT approach is resource and time-consuming while limiting the assessment of the interactions between the different operational factors. Also, their setup produced only a limited amount of biochar and bio-oil which restricted a full characterization of these products. Thus, these limitations and the use of a catalyst to suggest the operating conditions that maximize the mass yield of OPT bio-oil are explored in the present work.

The influence of the temperature, residence time, and catalyst dosage on the mass yields of the products from HTL of OPT were evaluated experimentally. This was done by using a half-fractional experimental design considering two levels for each process variable (Kleppmann, 2014; Antony, 2014). In addition, a thorough characterization of the properties of the bio-oil and biochar using different characterization techniques is provided. The experimental approach aims to provide a deeper understanding of the potential of OPTs to increase the circularity of the oil palm industry. Furthermore, the mathematical models result of the half-fractional experimental design are a potential stepping stone for those looking to perform techno-economic assessments of HTL of OPT.

2. Materials and methods

2.1. Experimental design

A two-level half-fraction experimental design was implemented to assess the effects of temperature, reaction time, and catalyst dosage on the distribution of the phases obtained from HTL of OPTs. This experimental design was built considering the details shown in Table A.5 and using Minitab® 21.1.1 (64-bit).

The generators and factor levels were assigned in the following manner: temperature (A) from 260 to 300˚C, residence time (B) from 15 to 60 min, and catalyst dosage (C) from 0 to 5 wt% with respect to the dry biomass content. The ranges for the temperature, residence time, and catalyst dosage were based on the typical operating conditions reported in the literature for HTL of OPTs (Muda et al., 2019) and different lignocellulosic biomass feedstocks (Madsen and Glasius, 2019). Based on the combinations of factors and their duplicates, the tests were randomly ordered as shown in Table 1. The settings for creating the 2^{3-1} experimental design are presented in Supplementary Information Table A.5.

Data retrieved from the experimental campaign were fitted to the linear model shown in Equation (1). This model considers the linear

Table 1
Summary of tests conducted according the 2^{3-1} experimental design.

Run order	Factors			Coded factors		
	Temperature - (A) [°C]	Time - (B) [min]	Catalyst - (C) [wt %]	Temperature	Time	Catalyst
1	260	15	5	− 1	− 1	+ 1
2	300	15	0	+ 1	− 1	− 1
3	300	60	5	+ 1	+ 1	+ 1
4	260	60	0	− 1	+ 1	− 1
5	260	60	0	− 1	+ 1	− 1
6	260	15	5	− 1	− 1	+ 1
7	300	15	0	+ 1	− 1	− 1
8	300	60	5	+ 1	+ 1	+ 1

effect of the temperature (A), residence time (B), and catalyst dosage (C) combined with the interactions, according to the aliases (see Table A.5). The goodness of fit of each model was evaluated based on its coefficient of determination (r^2), *F*-value, and standard error of regression (SER). The statistical significance of each parameter was evaluated based on its *p*-value. Finally, a response surface was generated to represent the effect of each parameter and the combinations based on the generated model.

$$Y_i = \widehat{X_0} + X_A\widehat{A} + X_B\widehat{B} + X_C\widehat{C} \quad (1)$$

2.2. Sample preparation

The OPT samples were obtained from two plantations - members of GREPALMA - located in the northern and southern regions of Guatemala (see map in Fig. 1) to take into account any variations in chemical composition. The samples were provided in the form of blocks of about 2 kg of freshly felled OPT. Prior to shipment and experimentation in The Netherlands, the particle size and moisture content of the samples was reduced to comply with customs regulations from the European Union and meet technical requirements to reduce heat and mass transfer limitations. The particle size reduction was conducted at the University of the Valley of Guatemala (UVG) using a shredder (Trapp TR200) and a coffee grinder to reach a maximum particle size of 60 mesh (250 μm). As a second step, the samples were dried in a shelf dryer (Corbett Industries Model EC-404–6) up to a moisture content of about 15 wt%.

2.3. Reactor setup and experimental procedure

Prior to running an HTL experiment, the moisture content of the sample was determined according to NREL/TP-510–42621 procedure. Then, slurries of around 150 g were directly prepared in a pressurized 300-mL autoclave mini-reactor (Parr Instrument Company, IL., USA., Series 4560), using Milli-Q water as solvent such that the dried-biomass solid content was of about 15 wt%. In the case of the catalytic runs, the heterogeneous Ni/Si-Al catalyst (Sigma-Aldrich 208779) dosage was set to 5 wt% with respect to the biomass content on a dry basis (d.b.). This catalyst is highly stable (Guan et al., 2014) and has shown a significant increase in bio-crude production as a result of its catalytic activity in hydrogenation reactions (Scarsella et al., 2020). Further details and full characterization of the Ni/Si-Al catalyst can be found in Scarsella et al. (2020) and Guan et al. (2014).

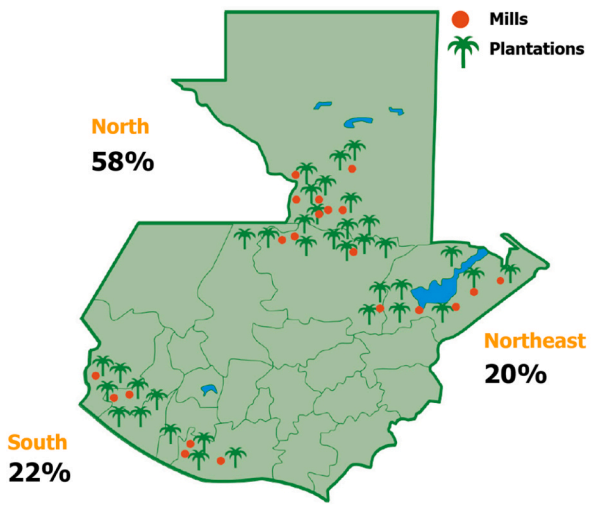

Fig. 1. Geographic distribution of oil palm plantations in Guatemala. Based on: 2021.

In order to ensure an inert atmosphere, nitrogen gas was injected into the reactor to vent the air out from the headspace of the vessel. This was followed by sparging nitrogen gas up to 1.4 bar(g). Then, the operating temperature was set along with a stirring speed of 150 RPM via the reactor controller. Once the residence time was completed, the reactor was cooled down from operating temperature to ambient temperature. Upon conversion of the OPT, the different phases containing the liquid and solid products were separated, extracted, and purified (Fig. 2).

First, the slurry and the aqueous phase from the reactor vessel were transferred into separate beakers. The reactor vessel, stirrer, and thermowell were rinsed with dichloromethane (DCM, Sigma-Aldrich). The solids still present in the aqueous phase were removed by vacuum filtration using a qualitative filter paper (Whatman™ No. 5). After filtrating the aqueous phase, the slurry with DCM was transferred to a Büchner funnel. The slurry and corresponding beaker were rinsed using DCM until the filtrate exhibited a light brown color. Then, the retained solids were vacuum-dried for 5 min and the filter cake (biochar) was transferred to a crucible for drying in a muffle furnace (Nabertherm 30–1300°C, Nabertherm GmbH, DE) at 105°C. Finally, the bio-oil was separated from the DCM-rich phase using a 250 mL separatory funnel. Using DCM additions, liquid-liquid extraction was conducted to purify the organic phase.

After performing the liquid-liquid extraction, the DCM was removed from the organic phase by vacuum rotary evaporation (Heidolph-VAP® Precision, Heildoph Instruments). The bio-oil was poured from the round flask into a pre-weighted vial and then stored at 4°C until further characterization. Vacuum rotary evaporation was also used to measure and remove water from the aqueous phase.

2.4. Product characterization

2.4.1. Elemental analysis and high heating value (HHV)

The elemental composition of the bio-oil (C,H,N,S) was determined using a varioMICRO CHNS analyzer, and the data was processed with varioMICRO V4.015 software (Elementar Analysensysteme GmbH, Langenselbold, DE). The HHV of both, bio-oil and biochar was determined according to ASTM standard D2015–00 using an adiabatic oxygen bomb calorimeter Model 1341 (Parr Instrument Company, IL., USA) coupled with a Parr 6772 calorimetric thermometer and controller. Enough oxygen was supplied up to 27 bar(g) into the pressurized vessel containing samples of about 1.0 g of biochar, and 0.5 g of bio-crude oil. In addition, the HHV of the bio-oils and biochars were estimated by considering the elemental composition and implementing the Boie and Gaur & Reed correlations (See equations A.3 and A.4, respectively).

2.4.2. Inductively coupled plasma - optical emission spectroscopy (ICP-OES)

The biochars (0.1 g per sample) were digested in 10 mL of Aqua regia on a heat plate. Data on elemental content was acquired using a Spectro-Arcos EOP combined with Spectro Smart Analyzer Vision software. Detailed results of ICP-OES are reported in Supplementary Information (See Fig. A.1 and Table A.7).

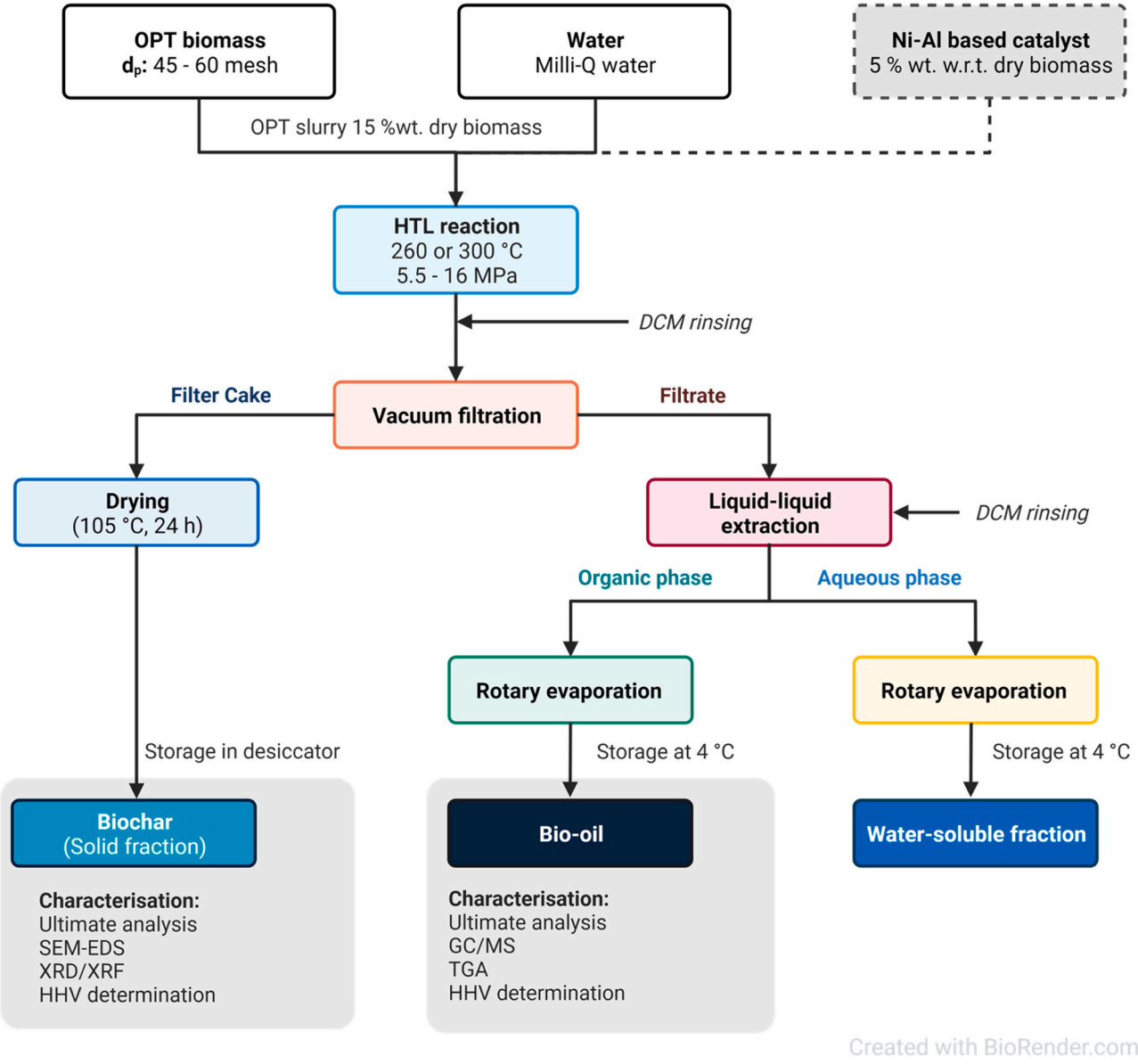

Fig. 2. Schematic for (non-)catalytic hydrothermal liquefaction process in a batch lab-scale reactor, product separation, and purification for further characterization.

2.4.3. Gas chromatography - mass spectroscopy (GC-MS) of bio-oils

The samples for GC-MS analysis were prepared by diluting the bio-oil with 2-propanol (VWR Chemicals) on a 1:10 mass ratio. Then, this fraction was filtered using a syringe 0.2 μm PTFE filter (Whatman™ Puradisc 13). The GC-MS was carried out using an Agilent 8890 gas chromatograph (Agilent Technologies, Wilmington, USA) equipped with an HP-5MS column from Agilent (model: USR577054H), a split-splittles liner (Agilent 5190–2295) and coupled with both mass spectrometer detector. The detailed routine for GC-MS can be seen in Brandi et al. (2023), (2021).

2.4.4. Water content of bio-oils

The water content of the bio-oil was determined via Karl-Fischer Titration using an 831 KF Coulometer (Metrohm, Herisau, Switzerland). For this, a sample of bio-oil of around 1 mL was injected into the titration vessel. Once the endpoint was reached, the value of the water content was recorded along with the mass of the sample being injected.

2.4.5. X-ray diffraction (XRD) and X-ray fluorescence (XRF) of biochars

All XRF spectra were measured with a WD-XRF spectrometer Axios^{mAX}-Minerals and processed with the analytical software SuperQ5.0i both supplied by PANalytical (Almelo, The Netherlands). XRD patterns were obtained using Bruker D8 Advance diffractometer Bragg-Brentano geometry Lynxeye position sensitive detector and Cu Kα radiation with the following measurement method: Diffraction patterns were scanned with 2θ range of 5° to 80°, step size 0.020° 2θ, and counting time per step 1.25 s.

2.4.6. Scanning electron microscopy coupled with energy dispersive spectroscopy (SEM-EDS) of biochars

The surface morphology of the biochar was analyzed with a JEOL IT100 Scanning Electron Microscope (SEM) equipped with an Energy dispersive X-ray spectroscopy (EDS) detector in low vacuum mode. SEM images were recorded using a backscattered electron detector in a compositional mode with an accelerated voltage of 10 kV and beam current of 65 pA. The results were extracted using the InTouchScope™ software and are expressed as atom percentage.

3. Results and discussion

3.1. Product distribution and response surface for HTL conversion

The focus of this study was to compare the product distribution between catalytic and non-catalytic HTL of OPT. The average mass yields for each HTL phase along with their standard deviations obtained for the half-fraction design of experiments approach are summarized in Table 2. The procedure for calculating the mass yields is provided in the supplementary information (Appendix A).

As can be seen from Table 2, the biochar yield is increased by higher temperature or longer residence time which is mainly attributed to the repolymerization of lignin (Muda et al., 2019). On the other hand, maximizing the aqueous phase can be achieved through longer residence times in non-catalytic processes or shorter residence times in catalytic processes. The maximum bio-oil yield was obtained in the presence of catalyst with a mild treatment (i.e., lowest temperature and lowest reaction time) at 260˚C and 15 min. For both non-catalytic and catalytic routes, the gas and losses fractions increased significantly at higher temperatures. For the catalytic pathway, this phenomenon happens at a longer residence time. Furthermore, the highest bio-oil production falls within the reported range (i.e., from 10 wt% up to 30 wt%) by Muda et al., for HTL of OPT without a catalyst and with a distinct experimental setup.

By fitting the mass yields presented in Table 2 to the corresponding linear models, we obtained the coefficients and statistical parameters presented in Table 3.

As can be seen from Table 3, all of the models fit the experimental data with acceptable accuracy since the coefficient of determination (r^2) is more than 80% in all the cases. However, it can be seen that the model for the bio-oil fraction requires further improvement as it resulted in the lowest value for the r^2 and the largest p-value ($p \geq 0.05$). This suggests that some interaction terms (e.g., time - catalyst and temperature - catalyst) are relevant for accurately capturing their influence. From the mathematical models presented in Table 3, a set of response surfaces was produced, and each one of them is shown in Fig. 3. The plots are a tool for graphically identifying a potential optimum set of operational conditions, which maximize the yield of bio-oil.

From Fig. 3(a) it can be seen that the presence of catalyst (e.g., 5 wt% with respect to the biomass dry content in the slurry) favored the production of bio-oil at low temperatures. On the contrary, the higher the temperature, the lower the yield of bio-oil. It is worth mentioning that our results are in agreement with existing literature, indicating that short residence time and low temperature benefit similar trends as reported for the HTL of OPT fibers via the non-catalytic process (Muda et al., 2019).

With respect to Fig. 3(b), biochar yield is typically optimized by using low temperatures and longer reaction times. This set of conditions is achieved without the use of catalyst (c.f., Table 2). For the aqueous phase, it was established that the yield is almost independent of the residence time due to the quasi-perpendicularity of the trends observed in Fig. 3(c) and the value obtained for the residence time ($\widehat{B}$) factor (see Table 3). In any case, the lower the temperature, the higher the yield of the aqueous phase regardless of the reaction time. It is important to note that while maximizing the production of bio-oil, the production of the aqueous phase is increased. Thus, careful design of the operation at a larger scale is required to be able to handle the large amount of aqueous phase that evolves from this process.

Finally, the contour plot for gas yield and losses demonstrates that gas yield increases with temperature, and residence time has an impact on it. Such effects have been attributed to the decomposition of the bio-oil and biochar into liquid compounds and further into non-condensable gases boosted by the activity of nickel in hydrogenation and cracking reactions (Scarsella et al., 2020).

3.2. Optimization and validation of the linear models obtained for the different HTL products

The factor values obtained from linear modeling were optimized in order to maximize the bio-oil yield within the experimental range. For this, an optimization routine was implemented in Minitab® 21.1.1 (64-bit) using the `Response optimizer` and verified via a `Nelder - Mead` routine in Python. Table 4 presents the criteria used and predicted operating conditions to optimize the bio-oil response.

Fig. 4 shows a graphical representation of the contour plot of the response surfaces for the bio-oil yield when spanned over the evaluated range of temperature, residence time, and for three levels of catalyst dose (i.e., 0, 2.5, and 5 wt%). From the optimization results (Fig. 4), it can be seen that the optimum conditions for producing OPT bio-oil correspond to a process run at 260˚C for 60 min and 5 wt% catalyst load with respect to dry biomass content.

The results from the optimization method were validated by performing two additional experiments at the optimum conditions that maximized the bio-oil yield. Table 5 presents the average yield of the validation experiment for each of the HTL products along with the absolute and relative error of the linear models.

Table 5 shows that the models that accurately predicted yields were the ones for the biochar and aqueous phases ($<$ 5.0% relative error). However, the models for the bio-oil and gas phase & losses had poor correspondence with actual yields (c.f., SER values in Table 3). Therefore, this provides an indication that the linear model approach is not the best way to capture the dependency of the bio-oil yield as a function of temperature, residence time, and catalyst dosage.

3.2.1. Proximate analysis of raw OPT and biochar

Table 6 presents the mean moisture, volatile matter, fixed carbon, and ash content for raw OPT and biochar produced under different operational conditions using both catalytic and non-catalytic routes.

As can be observed from Table 6, the moisture content of raw OPT is 12.1% (d.b.), which is typically regarded as high for dry thermochemical processes like pyrolysis ($\leq$10 wt%) (Abnisa and Wan Daud, 2014) (For HTL, a feedstock with a high moisture content is advantageous because less solvent would be required during the process. The ash content of Guatemalan OPT is higher than the range of values reported in literature (2.07–5.53 wt%), which explains the high biochar yields obtained for the evaluated operational conditions. With respect to the biochar, all samples have a significant ash content, regardless of the operational conditions. Biochars with high ash content have been linked to higher pH values which have proved useful for acidic soil improvement but are associated with low specific surface areas and greater amounts of PAHs and trace metals (Tomczyk et al., 2020). The volatile matter of biochars decreased with increasing temperature (300˚C) or prolonged residence

Table 2
Summary of product distribution results from tests conducted according the 2^{3-1} experimental design.

Test	Factors			Yields			
	Temperature [˚C]	Time [min]	Catalyst [wt%]	Biochar [wt%]	Aqueous [wt%]	Bio-oil [wt%]	Gas & losses [wt%]
I	260	15	5	23.48 (0.08)	35.21 (0.14)	26.77 (3.60)	14.55 (3.67)
II	300	15	0	28.66 (0.55)	26.06 (0.84)	16.45 (3.79)	28.82 (5.18)
III	300	60	5	21.96 (0.44)	23.84 (0.59)	23.40 (0.09)	30.80 (1.12)
IV	260	60	0	31.59 (0.20)	34.43 (0.37)	23.03 (0.47)	10.95 (1.05)

Table 3
Coefficients and statistical parameters for the lineal models of mass yields for products from HTL of OPT-derived biomass.

Parameter	Biochar		Aqueous		Bio-oil		Gas & losses	
	Value	*P*-Value	Value	*P*-Value	Value	*P*-Value	Value	*P*-Value
X_0	26.420	3.56E-09	29.884	1.07E-08	22.414	1.74E-05	21.279	5.09E-05
$\widehat{A}$	− 1.110	0.001	− 4.934	1.43E-05	− 2.486	0.055	8.529	0.002
$\widehat{B}$	0.353	0.054	− 0.751	0.018	0.801	0.436	− 0.404	0.744
$\widehat{C}$	− 3.703	9.17E-06	− 0.359	0.139	2.671	0.045	1.391	0.295
r^2	0.9955		0.994		0.8022		0.9335	
F-value	295.12		220.79		5.41		18.72	
SER	0.369		0.550		2.624		3.265	
p-value	3.79E-05		6.74E-05		0.068		0.008	

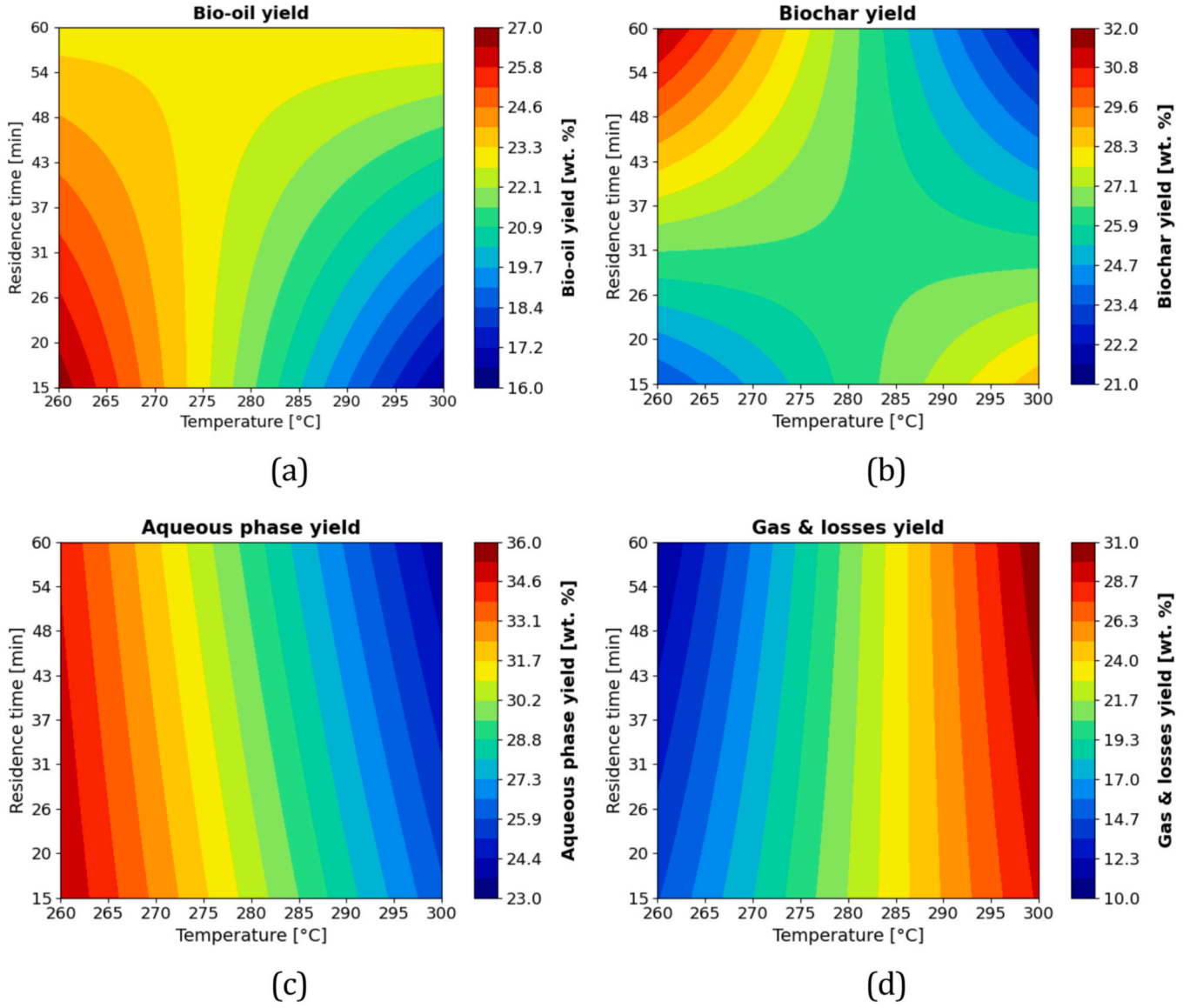

Fig. 3. Contour plots of the response surfaces for predicting the mass yields of a) bio-oil, b) biochar, c) aqueous phase, and d) gas and losses obtained under different operational conditions given the design generator (C = AB).

times (60 min). The biochar produced at 260˚C, 60 min, and no catalyst, has the highest fixed carbon content which might be beneficial for solid fuel applications.

3.3. Characterization of HTL products

In this section, an overview of the composition and properties of the bio-oil, aqueous, and biochar phases obtained upon HTL of OPT samples is provided. First, the elemental composition and energy content of bio-oil and biochar are given. Then, the composition of the bio-oil by gas

Table 4
Initial values and proposed solution for the optimization routine.

Variable	Unit	Initial value	Coded value	Prediction	Coded prediction
Temperature	°C	275	− 0.25	260	− 1.0
Time	min	25	− 0.56	60	1.0
Catalyst	wt %	2.5	0.0	5	1.0

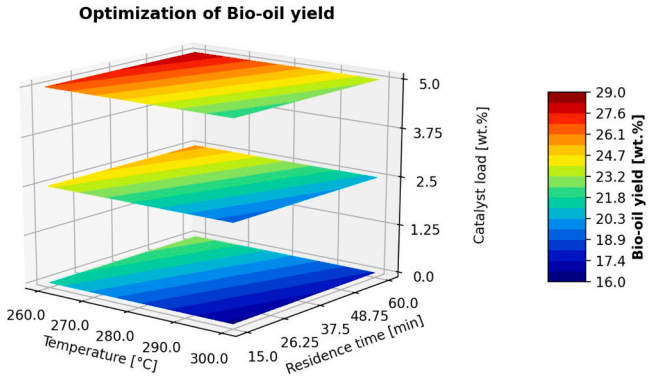

Fig. 4. Contour plots for the estimated bio-oil yield for three different doses of catalyst (i.e., 0, 2.5, and 5 wt%) using Eq. (1).

Table 5
Estimated and actual responses from the optimization of the bio-oil yield.

Test	Yields [wt%]			
	Biochar	Aqueous	Bio-oil	Gas & losses
Model prediction	24.18	33.71	28.37	13.74
Experimental validation[a]	24.97 (0.25)	32.04 (1.00)	22.42 (0.65)	20.57 (1.39)
Absolute error of the model	0.79	− 1.67	− 5.95	6.83
Relative error of the model	3.27%	− 4.95%	− 20.97%	49.71%

[a] Values in parenthesis correspond to the standard deviations of duplicates

Table 6
Proximate analysis for raw OPT and biochar samples.

Sample[a]	Moisture [wt% (d.b.)]	Volatile matter [wt% (d.b.)]	Fixed carbon [wt% (d.b.)]	Ash [wt% (d.b.)]
raw OPT	12.10	69.55	11.82	6.53
BC-300–15–0	1.16	33.62	39.55	25.67
BC-260–60–0	1.32	35.92	41.83	20.93
BC-260–15–5	1.49	35.99	38.44	24.08
BC-260–60–5	1.80	32.97	38.87	26.36

[a] Specified in the following order: temperature, residence time, and catalyst loading.

chromatography. This is followed up by an analysis of the elements present in the aqueous phase. Finally, an inspection of the morphological properties of the biochar samples is presented.

3.3.1. *Elemental analysis of raw OPT, bio-oil and biochar*

Table 7 presents the elemental content (C, H, N, S, O) in wt% daf (dry ash free) basis along with the experimental atomic ratios (O/C, H/C, and C/N) of dry OPT, bio-oil (BOPT) and biochar (BC) produced at different operating conditions by (non-)catalytic HTL. Moreover, the water content of the produced bio-oil (BOPT) is provided.

Table 7 shows that the bio-oils had a significant increase in carbon content up to 66.20 wt% (daf), which was followed by a decrease in the oxygen content compared with the raw OPT. The carbon content of OPT bio-oils via HTL is in agreement with values reported by (Muda et al., 2019) and at least 72% higher than the carbon content of OPT bio-oils produced by pyrolysis (33–45%) (Terry et al., 2021; Yakub et al., 2015). The H content of the bio-oils was increased up to 9.34 wt% (daf) for the non-catalytic tests and up to 6.90 wt% (daf) for the catalytic runs. The N content of the bio-oils is within the range reported in the literature for OPT bio-oils produced by HTL and pyrolysis (0.01–1.78 wt%) (Terry et al., 2021; Yakub et al., 2015). The S content of bio-oils was reduced in the presence of catalyst. The bio-oil with the lowest S content (0.16 wt %) corresponds to the test at 260°C, 60 min, and 5% catalyst. This is crucial since all of these bio-oils might adhere to existing regulations that are now in place for transportation purposes. For example, with the IMO regulations for fuel oils intended for maritime applications - the upper limit is 0.5 wt% S (Vermeire, 2021).

Compared with other thermochemical processes, the yields of OPT bio-oil from HTL (16–27 wt%) are less than those from pyrolysis (31–34 wt%) (Yakub et al., 2015). This might be attributed to high ash content in the parent feedstock (Table 6). Similar behavior was reported by (Muda et al., 2019), when comparing OPT bio-oil with raw spruce wood bio-oil produced via HTL.

Despite HTL produces less bio-oil than pyrolysis, pyrolysis of OPT requires higher temperatures (600°C), and the water content of OPT pyrolysis oils (41–43 wt%) (Yakub et al., 2015) is one order of magnitude higher than OPT bio-oils produced by HTL (< 0.70 wt%, Table 7). As a result, if HTL bio-oils require pretreatment, it will be far less than pyrolysis bio-oils in order to comply with existing regulation. For example, according to the ISO-8217 2010 Fuel Standard for marine residual fuels (Vermeire, 2021), the maximum limit of water content for marine fuels is 0.5 wt%. Furthermore, OPT bio-oils from HTL have significantly less water content than pyrolysis bio-oils from other type of palm oil residues (52–68 wt%) (Abnisa et al., 2013; Palamanit et al., 2019) and from HTL bio-oils from pine, microalgae and sewage sludge (12–17 wt%) (Jarvis et al., 2018).

For biochar, the carbon content of the different samples increased up to 25% (55.70 wt%) compared with the parent biomass. On the other hand, the N-content of the biochars slightly increased by 13% compared with the parent biomass in the presence of catalyst. However, this slight increase in N-content resulted in a significant decrease of the C/N ratio up to about 42% with respect to the raw OPT (See Table 7). The C/N ratio helps to predict whether soils will immobilize or mineralize N upon decomposition (Phillips et al., 2022). For biochar, it has been established that a crucial C/N ratio for horticultural purposes ranges from 20 to 32 (Sullivan and Miller, 2001). Based on this criteria, OPT biochars via HTL will induce N-immobilization, thus becoming unavailable to crops by microbial consumption (Brewer and Brown, 2012), except for BC-260–60–5. For S, the S content of all biochars was barely modified except for BC-260–60–5. This could indicate that longer times in the presence of catalyst results in sulfur fixation to the biochar rather than in the bio-oil. The OPT biochars also comply with the EU regulations for solid fuels, which demand the S-content to be < 2 wt%.

In Fig. 5, the Van Krevelen plot including the raw feedstock (OPT), biochar (BC), and bio-oil (BOPT) is depicted to compare the degree of aromaticity and carbonization of the different samples and literature (Zhang and Brown, 2019). For comparison purposes, Fig. 5 includes the zones and points corresponding to stages of the carbonization process, and some fossil-derived fuels.

After HTL conversion, the biochar and bio-oil fractions exhibit a reduction of the O/C and H/C ratios compared with the parent biomass. This is the result of the dehydration, decarboxyation, and decarbonylation reactions occurring during the HTL process (Kim et al., 2011). These reactions mainly cause a significant reduction in the O-content and enrich the C-content.

With respect to the bio-oils, the bio-oils produced via the non-catalytic route showed similar H/C and O/C ratios and are closer to Diesel fuel. On the other hand, the ones produced via the catalytic route

Table 7
Results from ultimate analysis, atomic ratios, and moisture or water content for dry OPT, biochar, and bio-oil produced at different operating conditions.

Sample[a]	Content [wt% daf]					Atomic ratios			Moisture
	C	H	N	S	O[b]	O/C	H/C	C/N	[wt%]
OPT	44.46	5.62	0.85	0.33	48.75	0.82	1.50	55.30	12.10
BC-300–15–0	55.70	4.34	1.21	0.39	38.38	0.52	0.93	53.68	1.16
BC-260–60–0	54.93	4.03	1.27	0.30	39.48	0.54	0.87	50.44	1.32
BC-260–15–5	52.49	4.57	1.69	0.36	40.90	0.58	1.04	36.22	1.49
BC-260–60–5	50.13	4.27	1.81	0.42	43.38	0.65	1.01	32.30	1.80
BOPT-300–15–0	66.20	9.17	0.51	0.44	23.69	0.27	1.65	151.93	0.67
BOPT-260–60–0	65.31	9.34	0.23	0.24	24.89	0.29	1.70	340.07	0.13
BOPT-260–15–5	57.59	6.21	0.60	0.18	35.44	0.46	1.28	113.12	0.02
BOPT-300–60–5	64.67	6.90	1.01	0.18	27.26	0.32	1.27	75.19	0.69
BOPT-260–60–5	62.94	6.70	0.86	0.16	29.35	0.35	1.27	85.44	0.67

[a] Specified in the following order: temperature, residence time, and catalyst loading. [b] Calculated by difference. [c] The standard deviation for the results can be seen in Table A.3.

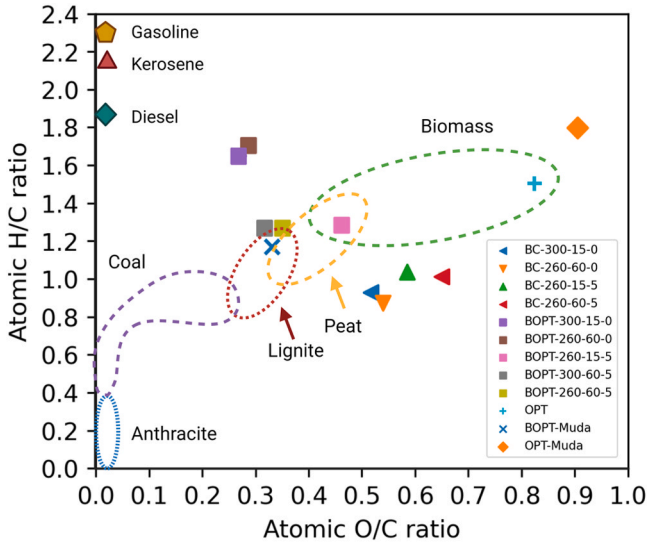

Fig. 5. The Van Krevelen plot of a raw sample of dried OPT, biochars (BC), and bio-oils (BOPT) after HTL reaction. The marked regions correspond to the coalification process - based on: de Jong (2015).

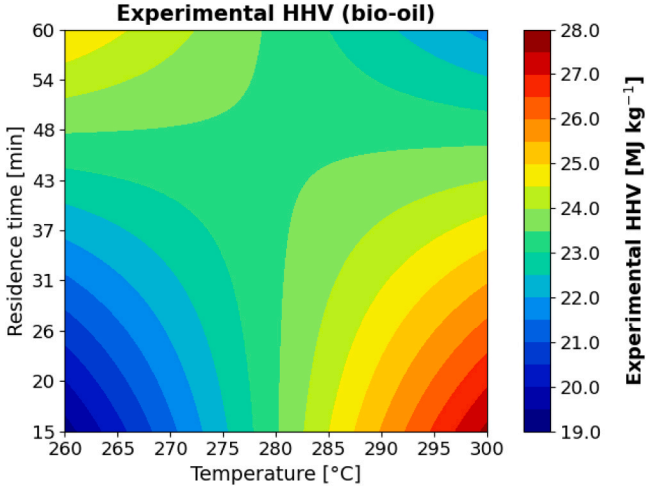

Fig. 6. Contour plot for the experimental HHV of the bio-oil fraction produced under different process conditions.

at 60 min are grouped in the region of lignite/aliphatic compounds (Danger et al., 2021) in the Van Krevelen diagram (Fig. 5). Such composition is similar to the one reported by Muda et al., for bio-oils produced at 250°C and 5 min with no catalyst (i.e., O/C: 0.33 and H/C: 1.24). When compared with OPT bio-oils produced through pyrolysis (Terry et al., 2021; Yakub et al., 2015), Guatemalan OPT bio-oils showed better quality if used as liquid fuels.

Regardless of the operational conditions, biochars are clustered (in triangles) in the same area of the Van Krevelen plot and indicate structural transformations result of the carbonization process under HTL conditions. Despite the fact that the biochar shows a certain degree of coalification, this was not sufficient to produce materials with properties similar to either peat, lignite, or gasification biochars (Del Grosso et al., 2022).

3.3.2. *High heating value (HHV) of raw OPT, bio-oil, and biochar*

Table A.4 shows the estimated and experimental HHV values for the different bio-oils and biochars. These values are key to evaluating whether the bio-oil and biochar produced from the experimental tests can be used as fuels. Furthermore, in Fig. 6 we provide a surface response plot based on the proposed linear model (Equation (1)) with coefficients calculated given the experimental HHVs of the bio-oils at different process conditions (See Table A.6).

The HHV values (Table A.4) of the bio-oils produced via the non-catalytic route (26.4 MJ kg^{-1} to 33.2 MJ kg^{-1}) are in agreement with the data reported by Muda et al., for bio-oils produced without catalyst and residence time of 5 min. Furthermore, as can be seen in Fig. 6, the HHV is higher for bio-oils produced via the non-catalytic route at higher temperatures along with shorter reaction times. Nonetheless, moderate HHV values are obtained for bio-oils produced in the absence of catalyst at lower temperatures and longer residence time. A comparison of the HHV plot in Fig. 6 with the plot for the bio-oil yields (Fig. 3(a)) suggests a potential trade-off between the yield and HHV of the bio-oil with respect to the use of the catalyst. In this sense, the catalytic HTL produces higher bio-oil yields but with lower energy content than the non-catalytic HTL. The HHV of BOPT-300–15–0 and BOPT-260–60–0 are comparable to the one of ethanol (29.85 MJ kg^{-1}). On the other hand, the ones obtained via the catalytic route (BOPT-260–15–5, BOPT-300–60–5, and BOPT-260–60–5) are expected to have an HHV similar to coal (23.97 MJ kg^{-1} w.b.) up to the one for dimethoxy methane - DMM- (25.67 MJ kg^{-1}). Furthermore, in average, Guatemalan OPT bio-oils have higher HHVs compared with pyrolysis oils (< 21.76 MJ kg^{-1}) reported by (Yakub et al., 2015; Sakulkit et al., 2020), except for the 28.04 MJ kg^{-1} OPT bio-oil reported by (Terry et al., 2021).

For biochars, it can be seen that an improvement in the HHV from 4% up to 63% with respect to raw OPT could be expected. The HHVs of biochars obtained from HTL of OPT are comparable to those biochars produced through wet torrefaction of OPT (17.84–26.84 MJ kg^{-1}) (Soh et al., 2023). This finding highlights the potential of HTL, as biochar derived from HTL is a by-product, yet possesses good quality. In contrast, wet torrefaction is oriented to exclusively produce biochar.

The higher HHVs were obtained for biochars produced in the absence of catalyst and short reaction times rather than the ones produced using catalyst. This could indicate that the longer the residence time, the most likely the biochar decomposes and gases evolve as Fig. 3(d) suggests. Additionally, the presence of catalyst might inhibit the re-polymerization reactions as they facilitate breaking the C-C bonds of organics (Scarsella et al., 2020). Regardless of this effect, the HHV is similar to the upper limit reported for peat and dry wood (i.e., 20.5 and 17.4 MJ kg^{-1}, respectively).

3.3.3. *Bio-oil composition: GC-MS analysis*

GC-MS analysis was carried out to identify the major components present in all bio-oils. Fig. 7 shows chromatograms indicating the percentage area of each of bio-oil.

Our results indicate that our bio-oils are mainly composed of phenolic compounds (phenol, 2,6-dimethoxy-phenol, 2-methoxy-phenol, 4-ethyl-2-methoxyphenol, vanillic acid), long-chain fatty acids (9-Octadecenoic acid or oleic acid), palmitic acid (n-Hexadecanoic acid), cyclic ketones (2-Methyl-2-cyclopenten-1-one) and carboxylic acids (Benzoic acid). These observations agree with previously reported bio-oil compositions from HTL of OPT (Quitain et al., 2015; Deris et al., 2006; Muda et al., 2019), especially regarding the phenols. Phenols are an important raw material for the production of chemicals such as dye, fuel additives, plastics, pesticides and resins (Sangthong et al., 2022). The bio-oil produced at 300˚C and 15 min without the catalyst is among the samples with the highest content of phenolic compounds along with BOPT-260–60–0 and BOPT-260–60–5. The composition of these bio-oils is correlated with high HHVs as presented in Table A.6.

In addition, for the same temperature (260˚C) and catalyst (5 wt%) dosage, an increase in the residence time from 15 min to 60 min increased the peak area (%) of phenolic compounds by 7% and reduced the peak area (%) of palmitic acid by 50%. The increase in phenolic compounds might be because longer residence times allow for more interaction between the OPT and catalyst, which increases the cracking of larger molecules. Compared with previous studies for OPT (Muda et al., 2019; Deris et al., 2006) or oil palm residues (Quitain et al., 2015),

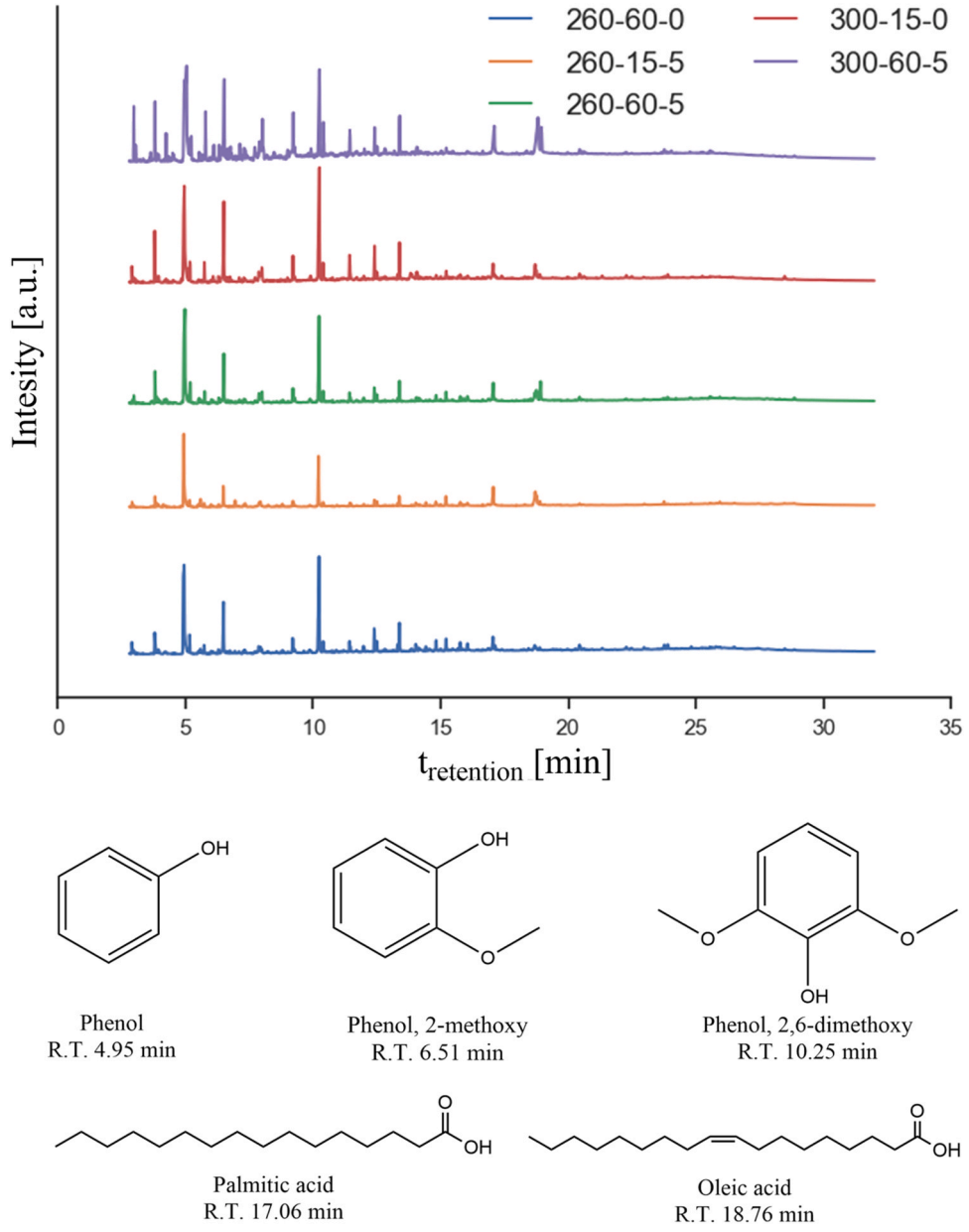

Fig. 7. Results from GC-MS analysis for different bio-oil samples produced via the (non-) catalytic process. The chemical structures and retention time of the major compounds are also presented in the figure.

we identified a relevant amount of free fatty acids such as palmitic acid (Fig. 7, 2–6%) in all bio-oils except in BOPT-300–15–0. The 50% reduction in the peak area of palmitic acid (BOPT-260–60–5) is attributed to the acid functionalities of the Ni/SiO_2-Al_2O_3, which hampers re-polimerization reactions and is responsible of the C-C cleavages (Scarsella et al., 2020). Furthermore, Ni/SiO_2-Al_2O_3 is known to have a high pore volume which allows a higher cleavage of the palmitic acid when penetrating into the pore of the support (Guan et al., 2014).

On the other hand, for the same residence time (60 min) and Ni/SiO_2-Al_2O_3 catalyst (5 wt%) dosage, an increase in the temperature from 260°C to 300°C reduces the amount of phenols by 25%. This experimental observation indicates that higher temperatures favor subsequent reaction of these compounds in the liquid phase into non-condensable gases. This is also supported by the fact that a more varied set of organic compounds were identified (Fig. 7) for the bio-oils produced at higher temperatures or longer residence times (i.e., BOPT-260–60–5 and BOPT-300–60–5). Furthermore, an increase in temperature from 260°C to 300°C favors the formation of fatty acids, i.e., oleic acid, and palmitic acid.

3.3.4. Composition of aqueous phase

The composition of trace elements present in the aqueous phase was determined by ICP-OES. The concentration (in mg/L) of different elements for aqueous fractions obtained at different operating conditions is shown in Fig. 8, and the respective values in Table 8.

Fig. 8 shows that Ca, K, Mg, and Cl are abundant in the aqueous phase since their concentration is in the 10^3 mg/L order of magnitude. This agrees with the fact that K and Cl have been proved to be transferred from solid particles to the aqueous phase upon hydrothermal processing (Lundqvist, 2016; Soh et al., 2022). Additionally, the Cl-content increases proportionally with respect to higher temperatures and longer residence times. This phenomenon is particularly evident when using the Ni-Al catalyst. The contents of Ni and Co increased when processing OPT by catalytic HTL. This can be attributed to the fact that water under subcritical conditions can extract nickel and aluminum ions (Wanta et al., 2020). Such ions are attributed to the catalyst (Ni-Al based) or scrap debris when collecting the slurry from the Hastelloy B2/B3 autoclave vessel. Such alloy has a major content of Ni and Mo (Parr Instrument Company, 2023). Regarding the content of Cu, a slight increase in the concentration is observed when employing the catalyst. Finally, the concentration of B, Fe, Mg, Mn, Na, Sr, S, and Si seems to be unaffected by the different operating conditions and the use of the catalyst.

3.3.5. Biochar XRF, XRD, and morphological (SEM-EDS) analyses

XRF measurements were carried out to evaluate the changes in the inorganic constituents composition of the raw-OPT and biochars from HTL. Here, the focus was on the operating conditions that resulted in the minimum (300−15−0) and maximum (260−15−5) bio-oil yield, as well as the experimental validation point (260−60−5). The results from the XRF analyses are provided in Fig. 9.

As can be seen from Fig. 9, a significant change in the major concentrations of oxides of Si, Fe, Mg, K, Cl, and Na is observed in the biochars. The C-content of the raw-OPT was identified as levoglucosan ($C_6H_{10}O_5$) which is the main constituent of lignocellulosic biomass, but for the biochar samples, the C-content was identified as elemental carbon rather than a polymer.

For SiO_2 and NiO, their content increased with higher residence times and temperatures. The Si, Al, and Ni oxides found in the biochars produced through the catalytic process are mainly attributed to the catalyst (Ni-Al-based catalyst). These elements may come from scrap debris when collecting the slurry from the autoclave vessel. The autoclave vessel is composed of Hastelloy B2/B3 which has a major content of Ni and Mo (Parr Instrument Company, 2023). This is confirmed by ICP-OES analysis (Supplementary Information Fig. A.1), where Ni and Mo are present in all biochars.

When lower temperatures and residence times were used, CaO and MgO were efficiently lowered. As for K_2O and Cl, a significant reduction was observed for the conversion of raw-OPT into biochar. This is due to hydrothermal processing is known to remove partially/completely K and Cl from the solid phase and transfer them into the aqueous phase (Lundqvist, 2016; Soh et al., 2022). For combustion processes, biochars are desired to have low contents of K as it can react with Si-forming silicates which are known to promote corrosion and other operational problems in boilers (Werther et al., 2000). The biochar (BC-260–60–5) corresponding to the catalytic test with the longest reaction time has the lowest K_2O content. The Cl content for the biochar derived from the non-catalytic test (BC-300–15–0) corresponds to a trace since the content (0.098 wt%) is lower than 0.1 wt%. Finally, sodium oxide (Na_2O) was absent in all biochars, which might indicate that this element was mainly transferred to either the bio-oil or aqueous phase. It is important to note that observations have been reported in which the Na content has been reduced to below the detection limit of the equipment (Jiang and Savage, 2017). Nonetheless, ICP-OES analyses (Supplementary Information Fig. A.1) indicate that Na is still present in all biochars but at mg/L level, < 1000 mg/L.

In order to complement the results of the XRF, XRD analysis (Fig. 10)

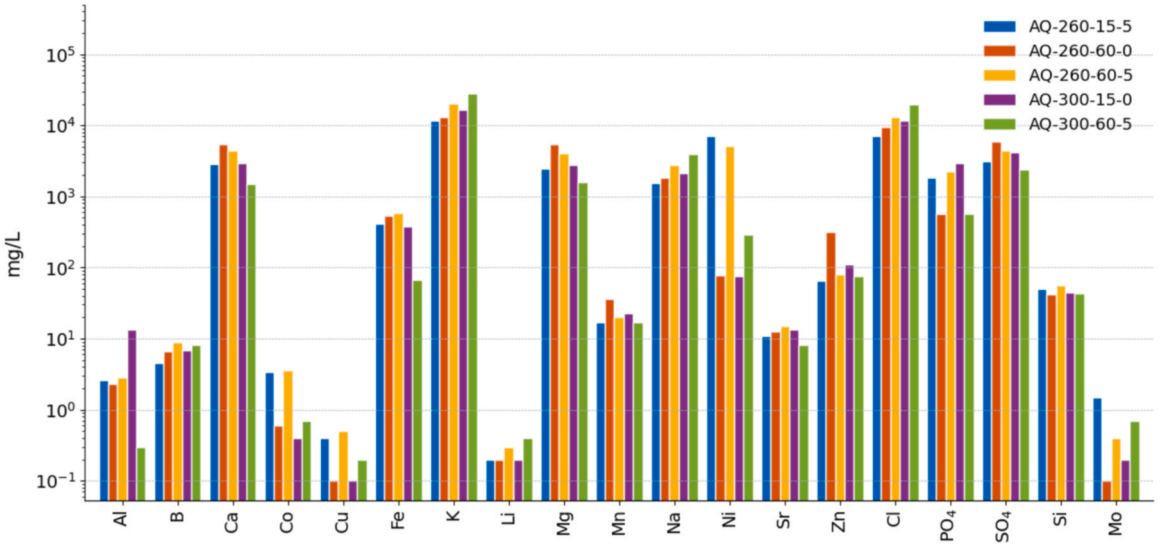

Fig. 8. Characterization of aqueous phase samples produced via HTL of OPT by ICP-OES analysis.

Table 8
Concentration of trace elements in aqueous phase samples.

Sample[a]	Al [mg/L]	B [mg/L]	Ca [mg/L]	Co [mg/L]	Cu [mg/L]	Fe [mg/L]	K [mg/L]	Li [mg/L]	Mg [mg/L]	Mn [mg/L]	Na [mg/L]	Ni [mg/L]	Sr [mg/L]	Zn [mg/L]	Cl [mg/L]	PO_4 [mg/L]	SO_4 [mg/L]	Si [mg/L]	Mo [mg/L]
AQ-260–15–5	2.6	4.5	2871.0	3.4	0.4	417.0	11660.0	0.2	2459.0	17.0	1537.0	7021.0	10.8	66.0	7007.0	1831.0	3097.0	50.0	1.5
AQ-260–60–0	2.3	6.7	5376.0	0.6	0.1	533.0	12921.0	0.2	5438.0	36.0	1831.0	77.0	12.5	317.0	9480.0	569.0	5988.0	42.0	0.1
AQ-260–60–5	2.8	8.9	4440.0	3.6	0.5	582.0	20496.0	0.3	4013.0	20.0	2809.0	5081.0	15.0	81.0	13128.0	2261.0	4478.0	56.0	0.4
AQ-300–15–0	13.5	6.8	2968.0	0.4	0.1	381.0	16658.0	0.2	2808.0	23.0	2138.0	75.0	13.5	111.0	11783.0	2982.0	4195.0	44.0	0.2
AQ-300–60–5	0.3	8.1	1489.0	0.7	0.2	67.0	28476.0	0.4	1592.0	17.0	3931.0	290.0	8.1	75.0	19669.0	567.0	2387.0	43.0	0.7

[a] Specified in the following order: temperature, residence time, and catalyst loading.

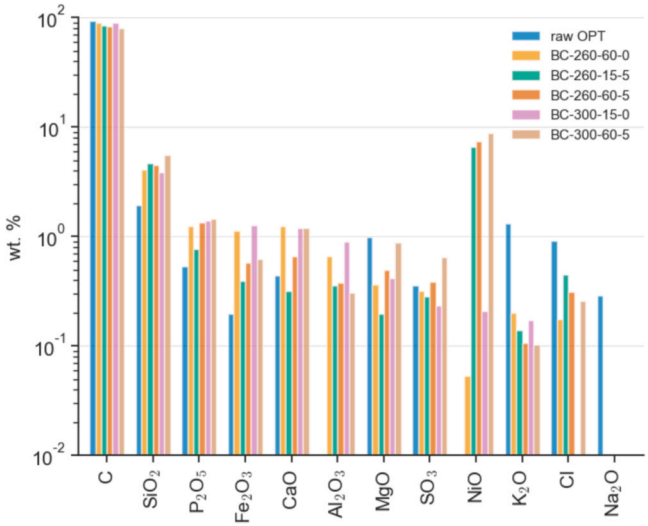

Fig. 9. Results from XRF analyses of different biochars for (non-) catalytic HTL. **Note:** Concentrations lower than 0.1 wt% were considered as traces.

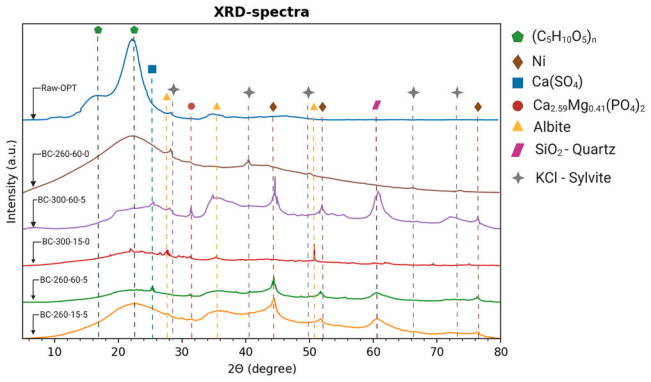

Fig. 10. XRD spectra for the raw OPT and biochar samples.

was performed. In this sense, the conversion of amorphous cellulose to crystalline cellulose is observed by the flattening of the peak at 2θ of 15.5˚ and 22.7˚ for BC-260–15–5. Meanwhile, the disappearance of these peaks in the spectra of BC-200–60–5 and BC-300–15–0 reflects the severity of the process and indicates the thermal decomposition of cellulose. On the other hand, the biochar obtained from the non-catalytic route at high temperature (BC-300–15–0) showed the presence of calcite ($CaCO_3$), albite ($(Na_{0.75}Ca_{0.25})Al_{1.26}Si_{2.74}O_8$), and quartz ($SiO_2$). The biochar obtained at a lower temperature (BC-260–60–0) exhibited the presence of sylvite (KCl). XRD spectra also confirmed the presence of Ni in the biochars produced with catalyst (i.e., BC-260–15–5, BC-260–60–5, and BC-300–60–5). Contrary to the XRF results, no clear peaks for Ni are observed in the biochar produced without catalyst (BC-300–15–0). Finally, the sample BC-260–60–5 showed crystal deposits of anhydrite ($CaSO_4$), along with sample BC-300–60–5 that also showed some crystals of whitlockite ($Ca_{2.59}Mg_{0.41}(PO_4)_2$).

Fig. 11 shows SEM images of the biochars produced at different operating conditions with corresponding EDS maps (square areas) and locations (numbers 1–3).

Results from SEM micrographs show that the biochars have a wide range of particle sizes and that there is a noticeable amount of inorganics near the surface. These inorganics mainly correspond to Si and Ni deposits according to EDS elemental analysis (Table 9). Such Si deposits mostly come from SiO_2 identified in the raw feedstock (see Fig. 9) and its concentration increased upon the carbonization and devolatilization during HTL, as confirmed by XRD results (Fig. 10). Furthermore,

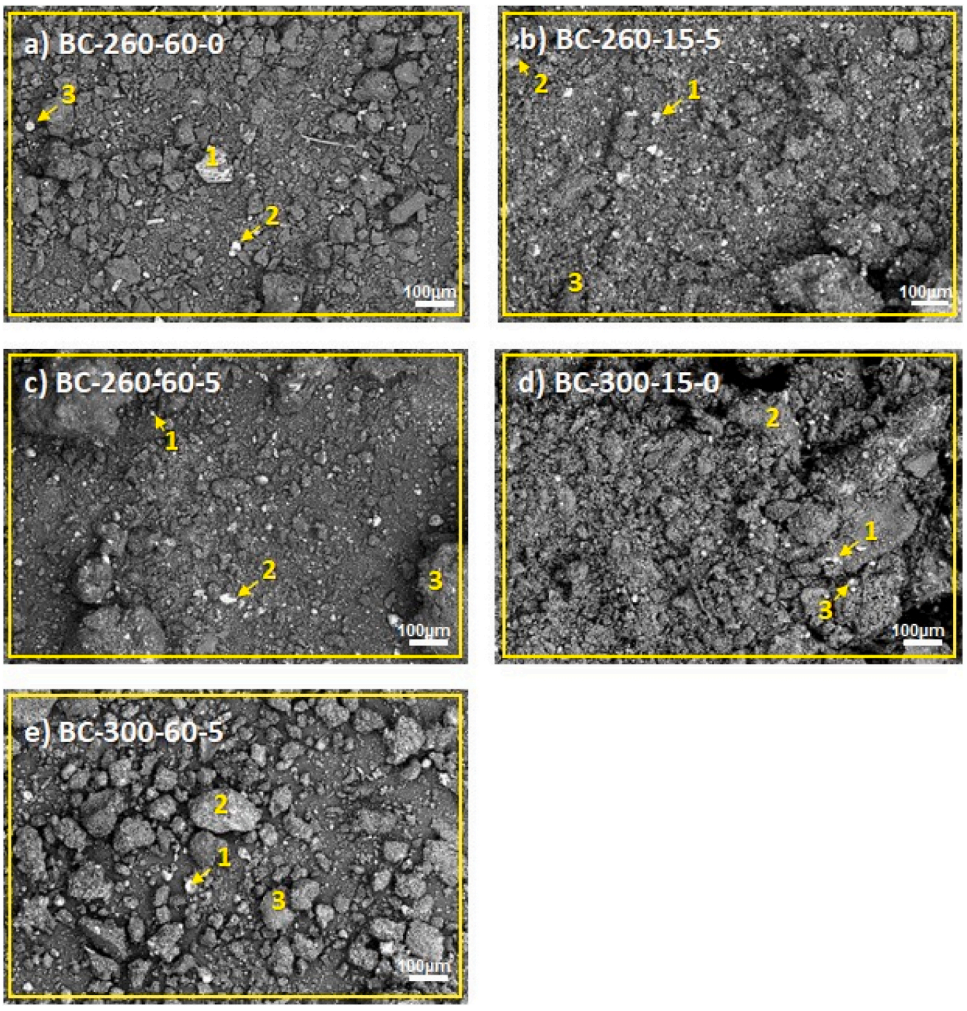

Fig. 11. Scanning electron microscope (SEM) images of the biochars after HTL. a) 260˚C for 60 min and no catalyst, b) 260˚C for 15 min and 5 wt% catalyst, c) 260˚C for 60 min and 5 wt% catalyst, d) 300˚C for 15 min no catalyst, e) 300˚C for 60 min and 5 wt% catalyst.

Table 9
Results from EDS elemental analysis for biochars obtained via HTL of OPT under different conditions (See Fig. 11).

Figure	Location	C [at%]	O [at%]	Si [at%]	Ni [at%]	Al [at%]	Na [at%]	Mg [at%]	S [at%]	P [at%]	K [at%]	Ca [at%]
10-a	Area	75.5	23.6	0.8	–	–	–	–	–	–	–	–
	1	56.1	35.2	4.5	–	3.2	–	0.5	–	–	0.6	–
	2	67.0	23.1	–	–	–	–	–	5.0	–	–	4.9
	3	63.0	26.2	5.3	–	3.2	1.0	–	–	–	–	1.3
10-b	Area	71.5	24.5	1.7	2.4	–	–	–	–	–	–	–
	1	71.5	21.8	1.6	5.1	–	–	–	–	–	–	–
	2	77.8	18.3	1.2	2.8	–	–	–	–	–	–	–
	3	78.1	17.8	1.5	2.5	–	–	–	–	–	–	–
10-c	Area	75.5	22.1	0.9	1.6	–	–	–	–	–	–	–
	1	84.2	14.6	0.5	0.7	–	–	–	–	–	–	–
	2	67.6	19.2	3.5	9.8	–	–	–	–	–	–	–
	3	78.5	19.5	0.4	1.5	–	–	–	–	–	–	–
10-d	Area	76.4	21.0	0.9	–	0.4	–	0.3	–	0.5	–	0.6
	1	75.5	22.7	1.2	–	0.6	–	–	–	–	–	–
	2	79.2	20.0	0.8	–	–	–	–	–	–	–	–
	3	70.5	24.9	0.8	–	–	–	–	–	1.8	–	2.1
10-e	Area	76.3	20.0	1.1	1.6	1.0	–	–	–	–	–	–
	1	75.0	18.0	1.0	4.2	0.5	–	0.4	0.8	–	–	–
	2	71.4	20.8	3.4	2.0	0.9	–	1.4	–	–	–	–
	3	76.5	19.5	1.0	1.9	0.6	–	0.4	–	–	–	–

according to the results from XRF (Fig. 9), XRD (Fig. 10), and EDS elemental analysis (Table 9), the catalyst used in HTL is the main cause of the bright particles found in the SEM images.

4. Conclusions

The following set of conclusions could be drawn from conducting a

half-fraction experimental design for the assessment of different operational variables on HTL of OPT:

- Using a 5 wt% catalyst dosage increased the bio-oil yield by 16% compared with the non-catalytic process for the same reaction temperature of 260˚C. Nonetheless, the bio-oils obtained without using a catalyst have higher HHVs (~ 31 MJ kg^{-1}) compared with the ones using a catalyst (~ 26 MJ kg^{-1}). This is attributed to the abundant presence of phenols which is generally higher in bio-oils produced without catalyst.
- The maximum biochar yield, 31.59 wt%, was obtained at 260˚C for 60 min without catalyst. On average, the HHVs of biochars exhibited an increase from 4% up to 63% compared with the raw feedstock. The biochars produced without catalyst and short reaction time showed the highest energy content (24.79 MJ kg^{-1}).
- We identified a potential trade-off between the mass yield of bio-oil and the HHV when using a catalyst. This trade-off requires further investigation such that the predictive model gets refined and the actual HHVs of the bio-oils are determined.
- A low concentration of Si, P, and Fe oxides was found in biochar with and without a catalyst, according to the analysis of its mineral composition and morphology. In the case of the SiO_2, white deposits were found on the surface of biochars. On the other hand, we observed a significant removal of alkali elements (i.e., Na and K) from the biochars. Interestingly, Al_2O_3 - absent in the raw feedstock - was added to the biochar no matter the processing route being used.

CRediT authorship contribution statement

Luis Cutz: Conceptualization, Methodology, Investigation, Data processing, Writing – original draft. **Héc**tor Maldonado: Conceptualization, Methodology, Investigation, Data processing, Writing – original draft. **Gamaliel Zambrano**: Resources. **Majd Al-Naji**: Investigation. **Wiebren de Jong**: Methodology, Supervision, Writing – review & editing.

Declaration of Competing Interest

The authors declare that they have no known competing financial interests or personal relationships that could have appeared to influence the work reported in this paper.

Data Availability

Data will be made available on request.

Acknowledgements

We thank Karen Rosales, Junior Barrios, and the partners from the Guild of Oil Palm Growers from Guatemala (GREPALMA, in Spanish) who kindly provided the OPT samples. We thank the members of the students' association of the Chemical Engineering Department of the University of the Valley of Guatemala - who preconditioned the samples prior to shipment to the Netherlands. We thank Ruud Hendrikx for conducting the XRD and XRF analyses at the Materials Science Engineering Department of the Delft University of Technology. Finally, we thank Dr. Wenze Guo and Ing. Michel van den Brink from the Process & Energy Department of the Delft University of Technology for welcoming the project and providing resources and support for its execution.

Appendix A. Supporting information

Supplementary data associated with this article can be found in the online version at doi:10.1016/j.indcrop.2023.117552.

References

Abnisa, F., Arami-Niya, A., Wan Daud, W.M.A., Sahu, J., Noor, I., 2013. Energ. Convers. Manag. 76, 1073–1082.
Abnisa, F., Wan Daud, W.M.A., 2014. A review on co-pyrolysis of biomass: An optional technique to obtain a high-grade pyrolysis oil. Energy Conversion and Management 87, 71–85. https://doi.org/10.1016/j.enconman.2014.07.007.
Antony, J., 2014. In: Antony, J. (Ed.), Design of Experiments for Engineers and Scientists. Elsevier, pp. 87–112.
Brandi, F., Antonietti, M., Al-Naji, M., 2021. Green Chem.
Brandi, F., Pandalone, B., Al-Naji, M., 2023. RSC Sustain.
Brewer, C., Brown, R., 2012. In: Sayigh, A. (Ed.), Comprenhensive Renewable Energy. Elsevier.
Castellanos, M.P., Imeri, L.M., Morfín, P.I., Méndez, P., Súchite, D., Maldonado, H., Piedrasanta, J. Estudio técnico y evaluación económica de la pirólisis de estípite de palma africana Deli x AVROS a nivel laboratorio y su escalamiento, Spanish, Bachelor Thesis, Universidad del Valle de Guatemala, 2017.
Cutz, L., Tomei, J., Nogueira, L., 2020. Energ. Policy 145, 111769.
Danger, G., Vinogradoff, V., Matzka, M., Viennet, J.-C., Remusat, L., Bernard, S., Ruf, A., d'Hendecourt, L.L.S., Schmitt-Kopplin, P., 2021. Nat. Commun. 12, 3538.
Del Grosso, M., Cutz, L., Tiringer, U., Tsekos, C., Taheri, P., de Jong, W., 2022. Fuel Process. Technol. 235, 107347.
Deris, R.R.R., Sulaiman, M.R., Darus, F.M., Mahmus, M.S., Bakar, N.A., 2006. In: Som, M., Veluri, M., Savory, R., Aris, M., Yang, Y. (Eds.), Proceedings of the 20th Symposium of Malaysian Chemical Engineers (SOMChE 2006), 19 - 21 December 2006. University Publication Center (UPENA), pp. 245–250.
Durak, H., 2023. Processes 11, 7.
Fleiss, S., Parr, C.L., Platts, P.J., et al., 2023. Implications of zero-deforestation palm oil for tropical grassy and dry forest biodiversity. Nat Ecol Evol 7, 250–263. https://doi.org/10.1038/s41559-022-01941-6.
Gollakota, A., Kishore, N., Gu, S., 2018. Renew. Sustsin. Energy Rev. 81, 1378–1392.
Guan, Q., Mao, T., Zhang, Q., Miao, R., Ning, P., Gu, J., Tian, S., Chen, Q., Chai, X.-S., 2014. J. Supercrit. Fluids 95, 413–421.
Helmer Pedersen, T., Conti, F., 2017. Waste Manag. 68, 24–31.
Hervas, A., 2021. Land Use Policy 109, 105657.
Jarvis, J.M., Albrecht, K.O., Billing, J.M., Schmidt, A.J., Hallen, R.T., Schaub, T.M., 2018. Energ. Fuel 32 (8), 8483–8493.
Jiang, J., Savage, P.E., 2017. Algal Res. 26, 131–134.
de Jong, W., 2015. In: de Jong, W., van Ommen, R. (Eds.), Biomass as a sustainable energy source for the future. John Wiley & Sons, Inc., pp. 36–65 ch. 2.
Kim, P., Johnson, A., Edmunds, C.W., Radosevich, M., Vogt, F., Rials, T.G., Labbé, N., 2011. Energy Fuel 25 (10), 4693–4703.
Kleppmann, W., 2014. Chem. Eng. Mag. 11, 50–57.
Lundqvist, P. Catalytic hydrothermal liquefaction of waste sludge - A pre-study with model compounds, Master's Thesis, Luleå University766 of Technology, 2016.
Madsen, R.B., Glasius, M., 2019. Ind. Eng. Chem. Res 58 (37), 17583–17600.
Meijaard, E., Brooks, T., Carlson, K.e.a., 2020. Nat. Plants 6, 1418–1426.
Mingorría, S., Gamboa, G., Martín-López, B., Corbera, E., 2014. Environ. Dev. Sustain. 16, 841–871.
Muda, N.A., Yoshida, H., Ishak, H., Ismail, M.H.S., Izhar, S., 2019. J. Wood Chem. Technol. 39 (4), 255–269.
Murphy, D., Goggin, K., Paterson, R., 2021. CABI Agric. Biosci. 2, 39.
Oettli, P., Behera, S., Yamagata, T., 2018. Sci. Rep. 8, 2271.
Ooi, L.-H. Palm pulverisation in sustainable oil palm replanting, 2004.
Parr Instrument Company.Materials of construction, n.d. (2023).
Palamanit, A., Khongphakdi, P., Tirawanichakul, Y., Phusunti, N., 2019. Investigation of yields and qualities of pyrolysis products obtained from oil palm biomass using an agitated bed pyrolysis reactor, 6 (4), 1065–1079. https://doi.org/10.18331/BRJ2019.6.4.3.
Phillips, C., Meyer, K., Garcia-Jaramillo, M., Weidman, C.S., Stewart, C.E., Wanzek, T., Grusak, M.A., Watts, D.W., Novak, J., Trippe, K.M., 2022. Biochar 9 (4), 15.
Quitain, A.T., Herng, C.Y., Yusup, S., Sasaki, M., Uemura, Y., 2015. Biofuels - Status Perspect.
Sakulkit, P., Palamanit, A., Dejchanchaiwong, R., Reubroycharoen, P., 2020. J. Environ. Chem. Eng. 8 (6), 104561.
Sangthong, S., Phetwarotai, W., Bakar, M.S.A., Cheirsilp, B., Phusunti, N., 2022. Ind. Crop. Prod. 188, 115648.
Scarsella, M., de Caprariis, B., Damizia, M., De Filippis, P., 2020. Biomass Bioenergy 140, 105662.
Soh, M., Khaerudini, D.S., Yiin, C.L., Chew, J.J., Sunarso, J., 2022. Clean. Eng. Technol. 8, 100467.
Soh, M., Mostapha, M., Chai, Y.H., Khaerudini, D.S., Phang, F.J.F., Chew, J.J., Loh, S.K., Yusup, S., Sunarso, J., 2023. Process Saf. Environ. 172, 1087–1098.
Sullivan, D., Miller, R., 2001. In: Stofella, P., Kahn, B. (Eds.), Compost utilization in horticultural cropping systems. CRC Press, pp. 95–120.
Teng, S., Khong, K.W., Che Ha, N., 2020. J. Clean. Prod. 274, 122901.
Terry, L.M., Li, C., Chew, J.J., Aqsha, A., How, B.S., Loy, A.C.M., Chin, B.L.F., Khaerudini, D.S., Hameed, N., Guan, G., Sunarso, J., 2021. Carbon Resour. Convers. 4, 239–250.
Tomczyk, A., Sokowska, Z., Boguta, P., 2020. Rev. Environ. Sci. Biotechnol. 19, 191–215.
United Nations Environment Programme.Converting waste oil palm trees into a resource, en, 2012.
2021 GREPALMA., 2021. agroindustria aceite de palma en Guatemala - estadísiticas socioeconómicas al año 2021.
Vermeire, M.B. Everything you need to know about marine fuels, en, 2021.

Wanta, K.C., Gunawan, W.T., Susanti, R.F., Gemilar, G.P., Petrus, H., Astuti, W., 2020. IOP Conf. Ser.: Mater. Sci. Eng. 742.
Werther, J., Saenger, M., Hartge, E.-U., Ogada, T., Siagi, Z., 2000. Prog. Energ. Combust. 26 (1), 1–27.
Williams, C.L., Dahiya, A., Porter, P., 2020. Bioenergy, 2nd ed. Elsevier,, pp. 5–44.
Yakub, M.I., Abdalla, A.Y., K.F.Y.S.A.I.S.C.J, 2015. Power Energy Eng. 03, 185–193.
Zhang, X., Brown, R.C., 2019. In: Brown, R.C. (Ed.), Thermochemical processing of biomass: Conversion into fuels, chemicals and power, 2nd ed. John Wiley & Sons, pp. 5–44.
Zhang, Y., 2010. In: Blaschek, H.P., Ezeji, T.C., Scheffran, J. (Eds.), Bioenergy, 2nd ed. Blackwell Publishing, pp. 5–44.